

# Thermorheological Testing and Modeling of a Bridge Slide-Bearing Elastomer

M.Eng. Johannes Köppl\*  
M.Sc.(hons) Michael A. Kraus \*\*  
Univ. Prof. Dr.-Ing. Ingbert Mangerig \*\*\*

\* University of German Armed Forces Munich, Germany, Institute of Structural Engineering,  
[johannes.koeppl@unibw.de](mailto:johannes.koeppl@unibw.de)

\*\* University of German Armed Forces Munich, Germany, Institute of Structural Engineering, [m.kraus@unibw.de](mailto:m.kraus@unibw.de)

\*\*\* Professor for Steel Construction, University of German Armed Forces Munich, Germany,  
[ingbert.mangerig@unibw.de](mailto:ingbert.mangerig@unibw.de)

## Abstract:

Due to the expected significant increase in total load of heavy goods vehicles as well as vehicle crossing numbers on the roads of the Federal Republic of Germany, sophisticated models for the design and computation of road bridges as well as their expansion joints are demanded. Furthermore great care is required for both, the load model in terms of correct or realistic Traffic Load Collectives as well as the establishing of physically and geometrically sensible computational models in terms of properties of the components. This paper hence deals with the experimental and thermorheological analysis of the elastomeric components of the swivel joist-expansion joint. The conduction of thermomechanical experiments as well as their results is described in detail, further analysis and evaluations of the data for material modeling purposes are then depicted. In an outlook the further incorporation of the constitutive equations together with their actual parameter values, which were derived in this paper, into an advanced Finite Element Analysis (FEA) model for the swivel joist-expansion joint is highlighted.

**Keywords:** Swivel Joist-Expansion Joint, Viscoelasticity, Prony Series, Mullins-Effect, Finite Element Analysis

## 1 Introductions and State of the Art

The infrastructure and especially the network of federal highways in Germany is one of the key factors of economic prosperity. Furthermore the network is also providing mobility to the inhabitants and thus ensures productivity as well as quality of life. Within this highway network, bridges are of particular significance. Recently conducted studies [1],[7],[8] claim, that a significant increasing in total load of heavy goods vehicles as well as vehicle crossing numbers on the roads of the Federal Republic of Germany could be observed, which is expected to further increase in future. Due to this trend, the realistic modeling of both, the traffic loads as well as the bridges and its components such as the expansion joints, is vital for an economic but reliable design.

Bridges vary their length due to temperature effects, which is compensated for by expansion joints. The expansion joints are installed transverse to the bridge's longitudinal direction at the beginning and at the end of the bridge to enable the vehicles' transition to the bridge abutments. Just in the specific case of an integral bridge structure expansion joints would not be needed. The preassigned gap width of an expansion joint depends on the relative displacement between the bridge and its abutment, where in general longer bridges require wider gap widths. In order to better understand and improve the fatigue behavior of the swivel joist expansion joint, which is represented in this paper, it is necessary to analyze the dynamic properties of the individual components in addition to the exact actions. Further investigations can then be carried out using the finite element method.

Up to now, expansion joints are modeled as single-degree-of-freedom (SDOF) or multiple- degree-of-freedom (MDOF) systems with constant parameter values for the springs and dashpots, [16][18]. The springs are modeled with a Hookean constitutive law and the damping behavior is assumed to be velocity- proportional or of the Rayleigh damping type. Expansion joint operate on site within an average air temperature ranges in the box girder from -5 to 25 degrees, c.f.[10] [11] However, the calculated design of the joint temperature is insensitive or calculated to the installation temperature of 10°.

The swivel joist-expansion joint under investigation within this paper consists of an elastomeric sliding key (made from natural rubber NR) and an elastomeric sliding bearing (made from chloroprene rubber CR). Polymer-based materials however show distinct hyperelastic and viscoelastic behavior, i.e. the material response to an arbitrary loading is geometrically nonlinear as well as temperature and time dependent. Within this paper, thus the thermomechanical realistic modeling of the elastomeric parts of a swivel joist-expansion joint is under consideration. Quasi-static and cyclic uniaxial compression tests as well as Dynamical-Mechanical-Thermal-Analysis tests were conducted on NR and CR specimen. The test result data and derived constitutive parameters are given within the context of this paper to provide more insight into the stiffness and damping characteristics of the elastomers NR resp. CR. This allows an accurate and realistic computation and design of expansion joints with these elastomers.

## 2 Description of the functionality of a swivel joist-expansion joint

In typical constructions of swivel joist-expansion joint the lamellas are transversally installed to the lanes. These lamellas are a kind of I-sections which are positioned in a previously determined interspace due to reasons of driving

comfort, acoustic emissions, and safety regulations. The head of these I-sections is built in a special geometric form to hold a waterproof sealing profile in between the I-sections. Those lamellas are supported via a slide bearing by swiveling cross bars which are arranged obliquely to each other. This oblique arrangement of the joists is the typical characteristic of swivel joist-expansion joints. So, these cross bars - or traverses - convey the vertical and horizontal traffic load from the lamellas into the expansion joint's substructure. To avoid the take-off of the lamellas resulting from their continuous effect over all three traverses, a clamping effect is induced by positioning prestressed elastomer slide bearing spring in two different locations. Within the center of the cross bar the spring elements are situated below the traverse connected to the lamellas by an L-shaped clamp causing an intended clamping effect. In contrast, within the bridge's superstructure as well as in the abutment, a joist box encased in concrete provides the support for the cross bar via a prestressed elastomer spring above it. These elastomer slide bearing springs consist of a non-reinforced elastomer component in the middle section between two bearing plates made from steel. Both, the supporting of the lamellas on the cross bars as well as the supporting of the traverse on its supports in the joist boxes is carried out in contrast to the previous non-reinforced via a reinforced elastomer slide bearing. Those supports consist of a reinforced bearing core. The reinforcement is achieved by two small steel plates and three elastomer layers positioned above, in between, and below which are connected to one another via a vulcanization process. Similar to the non-reinforced components, these are then provided with a lower and upper steel bearing end plate. For a detailed scheme of the entire construction refer to figure 1.

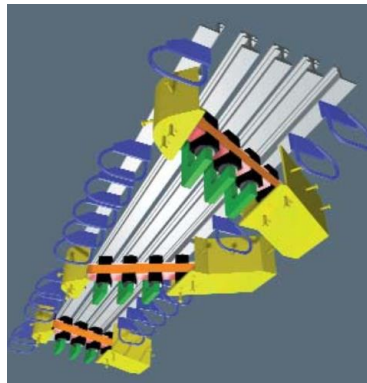


Figure 1: Swivel Joist-Expansion Joint, from [17]

This system with the prestressed elastomer components is necessary to maintain the position assurance of the lamellas and of the underlying traverse against slipping and rotating. This prestressing is introduced into the elastomer springs through vertical deformation. Additionally, these deformation are required for the installation of the springs above the cross bar.

The material of the sliding spring is natural rubber NR with vulcanized steel plates and of the reinforced sliding bearing it is chloroprene rubber CR.

### 3 Thermomechanics of Polymers

Polymeric materials show strong time and temperature dependent material behavior, c.f. [6] [16] [17] [23]. In the context of this paper only an introductory overview on the theory of hyperelasticity as well as large strain and linear viscoelasticity is given, further deductions and a more detailed description of the topic can be found in [3] and [4].

#### 3.1 Temperature dependent material behavior of polymers

Polymers can be classified under different aspects, the classification according to polymeric structure and mechanical behavior is of interest for the engineer-technical description [12], [2]. Depending on the stiffness-temperature behavior, polymers are classified into three main classes: thermoplastics, elastomers and duroplastics. Thermoplastic elastomers, in which elastic polymer chains are embedded in thermoplastic material, represent a subcategory, see [13], [14].

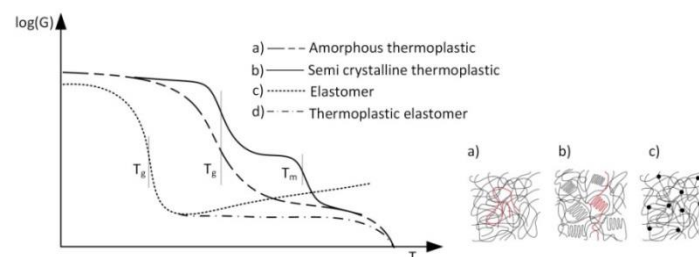


Figure 2: Temperature dependent behavior of polymeric interlayers according to [14]

In the temperature-stiffness-graph, c.f. Fig. 2, two characteristic areas of stiffness are visible, which are separated from each other by the glass transition area. Here, a significant decrease in stiffness, characterized by the glass transition temperature  $T_g$  is observed, cf. [13]. At temperatures below the glass transition temperature, the polymer is in a glass-like state with relatively high stiffness (energy-elastic range) whereas at temperatures above the glass transition temperature, the polymer behaves rubber-like with a relatively low stiffness (entropic elasticity). Thermoplastics (Figure 2a, b)) do not possess chemical molecular crosslinking, thus the stiffness decreases continuously until the melting point  $T_m$  is reached. Elastomers (Figure 2c)) are widely meshed and have a low increase in rigidity in the entropy-elastic range, which is dependent on the degree of cross-linking. Thermoplastic elastomers (Figure 2d)) can have physical cross-linking points (crystallites) in some areas, in which parts of different molecules are arranged relative to each other and thus form a regular crystal lattice. The two polymeric materials under investigation within this paper are NR and CR, which both belong to the group of elastomers. From [17] estimates the  $T_g$  of NR and CR can be given to  $T_{g,NR} \approx -60^\circ\text{C}$  and  $T_{g,CR} \approx -37^\circ\text{C}$ , based on these values and since the operating range is  $-5$  to  $+25^\circ\text{C}$ , the assumption of incompressible material behavior is justified.

### 3.2 Hyperelasticity

A configuration refers to the simultaneous position of all material points of the body  $\mathfrak{B}$ . Typically capital and lower case letters indicate, whether quantities belong to the initial (upper case letters, e.g.  $X = x_0; t = t_0; \mathfrak{B}_0$ ) or the current / deformed configuration (lower case letters, e.g.  $x_t; t > t_0, \mathfrak{B}$ ) respectively. The bijective deformation map  $\chi(X, t)$  defines the position within the current configuration of the particle  $P$  that originally occupied a given position  $P_0$  within the reference configuration. The deformation gradient  $\mathbf{F}$  describes this movement and is thus a second order tensor with

$$\mathbf{F} = \text{Grad}(\mathbf{x}_t) \quad (1)$$

For rubber-like materials above the Glass transition temperature  $T_g$  incompressibility is considered, which results in  $\det(\mathbf{F}) = J = 1$ . The left and right Cauchy-Green stretch tensors can be derived by:

$$\mathbf{b} = \mathbf{F}\mathbf{F}^T \quad \text{and} \quad \mathbf{C} = \mathbf{F}^T\mathbf{F} \quad (2)$$

The material models of hyperelasticity are usually formulated in the so called ‘Helmholz free energy’ (per volume)  $\Psi(\mathbf{b})$  or  $\Psi(\mathbf{C})$ , which is depending on the principal stretches  $\lambda_i$ , with  $i = 1, 2, 3$ . The basic assumption of constitutive models in hyperelasticity is, that the stress function of a thermoelastic material only depends on the applied deformation, the temperature  $\theta_0$  and the Gradient of the temperature  $\text{Grad}(\theta_0)$ , c.f. Eq. (2). It is possible to express the Helmholtz free energy in terms of the three invariants of the left and right Cauchy-Green stretch tensors, thus the Cauchy stress is expressed as:

$$\sigma_{\text{true}} = \frac{2}{J} \mathbf{F} \left[ \frac{\partial \Psi}{\partial I_1} \frac{\partial I_1}{\partial \mathbf{b}} + \frac{\partial \Psi}{\partial I_2} \frac{\partial I_2}{\partial \mathbf{b}} + \frac{\partial \Psi}{\partial I_3} \frac{\partial I_3}{\partial \mathbf{b}} \right] \mathbf{F}^T \quad (3)$$

Further simplifications of the notation of  $\sigma_{\text{true}}$  can be obtained using theorems of continuum mechanics, but these deductions are omitted at this point referencing [5] and Eq. (2) for further considerations. In the context of this paper, uniaxial compression tests were conducted. It is possible, to state analytical expressions for the deformation gradient  $\mathbf{F}$  as well as the left isochoric Cauchy-Green stretch tensor  $\mathbf{b}$  in terms of the stretch  $\lambda$  for the tested deformation mode:

$$\text{uniaxial compression:} \quad \mathbf{F} = \begin{bmatrix} \lambda & 0 & 0 \\ 0 & \frac{1}{\sqrt{\lambda}} & 0 \\ 0 & 0 & \frac{1}{\sqrt{\lambda}} \end{bmatrix} \quad \text{and} \quad \mathbf{b} = \begin{bmatrix} \lambda^2 & 0 & 0 \\ 0 & \frac{1}{\lambda} & 0 \\ 0 & 0 & \frac{1}{\lambda} \end{bmatrix} \quad (4)$$

The incompressible 2-parameter Mooney-Rivlin material model possesses two material constants  $C_{10}, C_{01}$ . The Cauchy stresses for the uniaxial compression experiment can be calculated via

$$\sigma_{\text{true,uniaxial}} = 2 \left( \lambda^2 - \frac{1}{\lambda} \right) \left[ C_{10} + \frac{C_{01}}{\lambda} \right] \quad (5)$$

### 3.3 Linear and Large Strain Viscoelasticity

Time- and temperature dependent behavior is modeled within the framework of the theory of viscoelasticity. In the following, it is assumed, that strains are small and the material behavior can be described with the theory of linear viscoelasticity (LVE). Within this theory the Generalized Maxwell-Model, c.f. Figure 3, and an associated Prony-series (Eq. (6) in the time and Eq. (7) in the frequency domain) can be used to describe time-dependency within the stress-strain-correspondence, [14]. The Prony-series  $E_R(t)$  consists of  $K$  decaying stiffness functions  $\hat{E}_k \exp(-t/\tilde{\tau}_k)$  with associated relaxation times  $\tilde{\tau}_k$  and an equilibrium stiffness  $E$ . Alternatively, the Prony-series can be formulated using the standardized modulus  $e_k = \hat{E}_k / E_0$ , where  $E_0$  corresponds to the Young’s modulus at time  $t = 0$ .

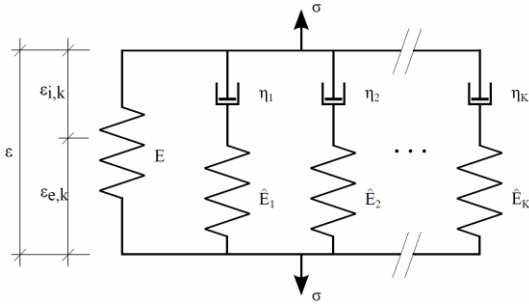


Figure 3: Generalized Maxwell-Model (left) and Prony-Series in the time and frequency domain (top and middle)

In addition to the time-dependence, the temperature influence has to be taken into account within the Generalized Maxwell element approach. For thermomechanical considerations, the glass transition temperature  $T_g$  is of special importance. The time and temperature dependence of polymers can be connected by the time temperature superposition principle (TTSP), c.f. [13] [2]. The TTSP states, that a stiffness curve at a given reference temperature can be used for predicting the stiffness over time for various temperatures by applying a shift to the reference curve. The reference curve is usually called Master Curve, c.f. [2], [13]. The Master Curve itself is constructed by isothermal measurements of the interlayer modulus at multiple temperatures and subsequent shifting by applying a shift factor  $a_T$  to the time at which the measurement is taken, c.f. Fig. 4. Analyzing the shift factors used at each particular temperature delivers the shift factor – temperature - relationship, which may possess a functional form such as the Arrhenius equation, the Williams-Landel-Ferry-Equation or polynomial form, c.f. [2] [10] [13]. The introduction of the TTSP into the Generalized Maxwell model in the frequency domain mathematically reads:

$$E^*(\omega) = E_\infty + \sum_{k=1}^K \hat{E}_k \frac{\xi^2 \cdot \tau_k^2}{1 + \xi^2 \cdot \tau_k^2} + i \sum_{k=1}^K \hat{E}_k \frac{\xi \cdot \tau_k}{1 + \xi^2 \cdot \tau_k^2} \quad (8)$$

Where  $\xi = a_T(T|T_{ref}) \cdot \omega$  is called the reduced frequency. The Prony parameters  $e_k$  (or  $\hat{E}_k$ ),  $\tilde{\tau}_k$  and  $E_0$  (or  $E$ ) have to be determined experimentally either via isothermal relaxation or creep experiments repeated at different temperatures or by using the dynamic-mechanical-thermal analysis (DMTA) within significantly less time compared to the relaxation / creep tests, c.f. [10],[14]. After having obtained the experimental raw data, the unknown Prony-parameters have to be fitted to the test data by means of a suitable identification method [10]. For the thermomechanical description of thermorheologically simple polymers, the Prony-series with an associated time-temperature superposition principle (TTSP) and a reference temperature  $T_{ref}$  is sufficient.

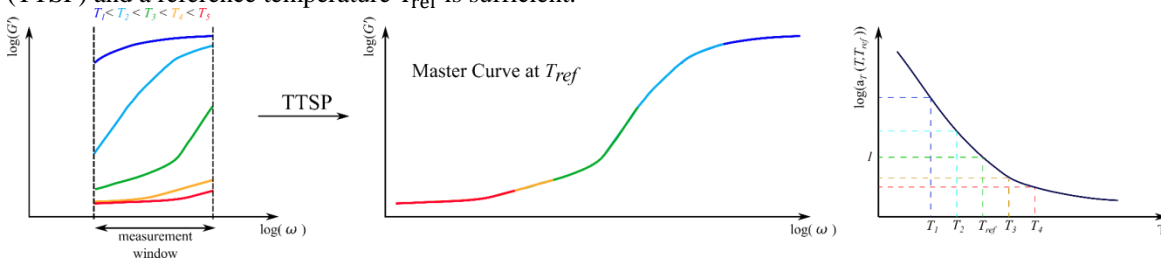


Figure 4: Master Curving Process (left) and shift factor - temperature relationship (right) in the frequency domain

The generalization of LVE to large strain viscoelasticity is given by using the Prony-series and introduction of the hyperelastic stress function  $\sigma_{hyper}(\epsilon)$ , c.f. Sec. 3.2, to finally obtain (for further deduction c.f. [5]) the following expression:

$$\epsilon(t) = \sigma_{hyper}(\epsilon(t)) - \int_0^t \dot{E}_R(t-s) \cdot \sigma_{hyper}(\epsilon(t)) ds \quad (9)$$

The evaluation of the experimental data will show, if it is necessary to incorporate hyperelastic or large strain viscoelastic theory for a correct constitutive description of the Natural rubber and Chloroprene rubber under investigation.

### 3.4 Damage and the Mullins Effect in Polymers

Mullins was the first to investigate the change in the mechanical properties (usually softening) of rubber-like materials

resulting from the first extension, thus this phenomenon is called ‘Mullin’s effect’, c.f. [15]. In order to account for the Mullin’s softening, [2],[5] proposed to penalize the elastic strain energy densities  $\Psi(b)$  (fitting a hyperelastic stress-strain response, c.f. Sec. 3.2) by a reducing parameter:

$$\Psi_d(b) = (1 - d)\Psi(b) \quad (10)$$

The Mullin’s softening effect in its simplest version can be explained easily for an uniaxial tensile or compression test.

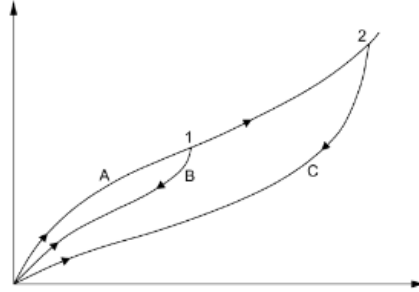


Figure 5: Schematic load-path under quasi-static loading in a stress-strain-diagram, from [5]

Considering Fig. 5, the test specimen is loaded along path *A* to level 1 and then relieved along path *B*. When loaded again, the sample now follows path *B* instead of path *A* to level 1. A loading beyond level 1 leaves the sample then follow path *A* again to step 2. The running of the sample on another path during the relief describes the damage *d* in the material. In sec. 4.1 of this paper, cyclical compression tests of the NR and CR bearings investigate the Mullin’s effect and its impact on the stiffness behavior of the swivel joist-expansion joint.

#### 4 Experimental Investigation

In this section, a detailed description of all conducted experiments is given. Investigations on the hyperelastic, Mullin’s and viscoelastic material behavior were carried out for the sliding spring (NR) and the sliding bearing (CR). The basis for all tests is the determination and specification of a proper load level. In order to find an appropriate loading, the force data of the crossing of a heavy goods vehicle within the swivel joist-expansion joint was analyzed. Based on the data, it was estimated a load spectrum of approx. 20 – 60 kN for the bearing, c.f. Fig. 6 left. The spring is exposed to significantly lower loads and is therefore subjected to a load spectrum of 15 - 25kN, c.f. Fig. 6 right. In Fig. 6, the force signal of the load cell is shown in the sliding spring (the figure shown here does not contain the maximum load of the spring but is instead used for a schematic representation). The curve clearly shows a smaller load in relation to the plain bearing, since the load cell shows the absolute force in the overall system, it is easy to see the change in preload force when a truck is driven over and thus the working range of the spring. These force operation limits serve as target loads for all further tests.

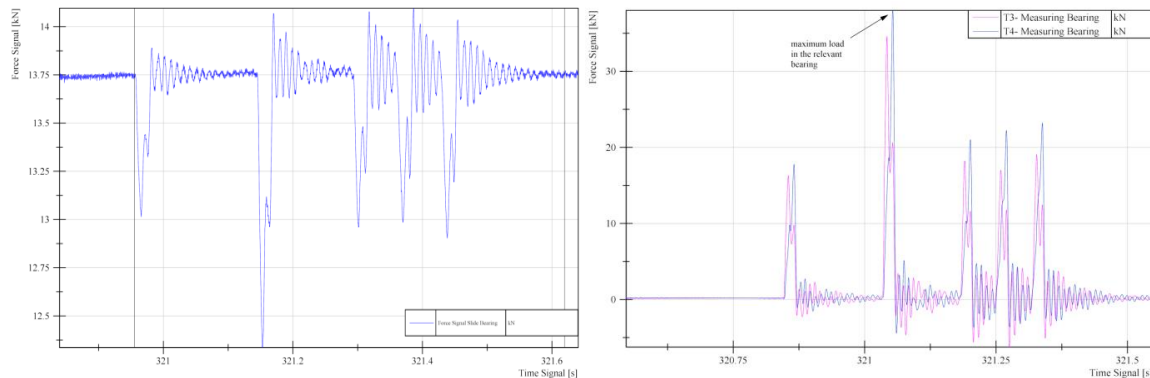


Figure 6: Change in prestress of the sliding spring due to overrunning a five-axle truck (left) and maximum measured load in a bearing due to crossing a five-axle truck (right)

##### 4.1 Quasi-Static Loading and Mullin’s Effect

Investigations w.r.t. the hyperelastic as well as stress-softening behavior was performed on real-size specimen in compression mode for both, the elastomer bearing and spring. The tests were operated force-controlled on a 100 kN electric cylinder of type “ZWICK” on three specimens at ambient conditions. All tests were performed with a rate of deformation of 1 mm/min. Care was taken to ensure that the introduction of the load into the system was close to reality. A steel tube with a diameter of 88.9 mm and a wall thickness of 12.5 mm was welded onto the force introduction ring, which is also used in reality. This construction is mounted to the load cell via a fitting pin connection. The test setup is depicted in Fig. 7.



Figure 7: Test setup of the quasi-static and cyclic investigations of sliding bearing and spring

The evaluation of the nonlinear (hyperelastic) stress-strain relation was simultaneously done with the testing for the Mullin's effect. As the correct estimation of the bearing stiffness's significantly influences the FEA results, the stiffness estimation from tests on a "virgin" specimen cannot be used because the material changes with each load cycle dependent in the maximum loading. This further means that, depending on the polymer and filler, the bearings must be subjected to a different number of loading and unloading cycles with the maximum stress occurring in the component until a constant material behavior is achieved, which is preconditioning the material. The Mullin's effect is therefore essentially dependent on the maximum stress in the component, because if a preconditioned specimen would be stretched / compressed beyond the currently applied maximum load, a further softening effect would be recognized.

The testing program comprises of two steps. The first test step is to run once 16 load cycles of increasing distortion amplitude as given in Tab. 1. The second step is to perform a continuous measurement over 10,000 compressive force cycles with constant distortion amplitude in order to assess the constant material behavior, c.f. Tab. 1.

Table 1: Parameter of quasi-static and cyclic investigations

Sample	sliding bearing NR	sliding spring CR
Sample geometry [mm]	Rectangle: $L \times W \times T$ : 150 x 100 x 50	Rectangle: $L \times W \times T$ : 150 x 100 x 57
Test equipment	electro mechanic testing actuator EZ100 Zwick	
Test mode	quasi-static and cyclic compression	
Test temperature [°C]	23	

The results depicted in Fig. 8 support clearly the presence of the Mullin's effect, which is more pronounced for the sliding spring (Fig. 8 right) compared to the sliding bearing (Fig. 8 left). Furthermore for the sliding spring (Fig. 8 right) a more severe hyperelastic stress-strain-relation can be observed in comparison of sliding bearing (Fig. 8 left). However, for engineering purposes one could draw the conclusion that the force-deformation relationship of both elastomers in their respective working range corresponds in good approximation to a straight line during loading, which permits a linear stiffness relationship for further work and the necessary investigations. Thus in the opinion of the authors of this paper a further incorporation of a hyperelastic constitutive law which furthermore accounts explicitly for the Mullin's effect is not necessary in case, the force operation windows are not left within the lifetime of the bearings.

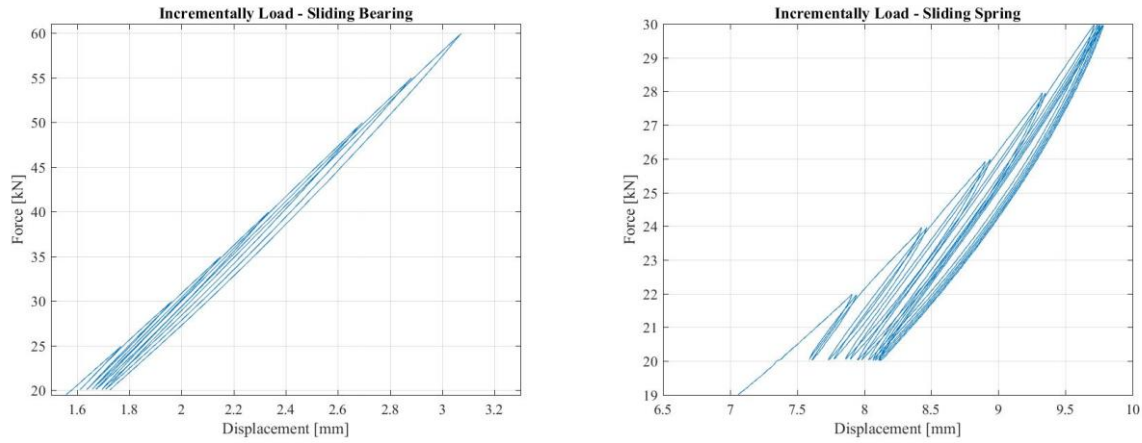


Figure 8: Force-displacement graphs for the sliding bearing (left) and the sliding spring (right) under cyclic step loading

The tests described below were now carried out on the preconditioned bearings. For this purpose, test samples for the small parts tests were cut out of the bearings and springs. To avoid heat input, the specimens were cut out with a water jet.

#### 4.2 Dynamic-Mechanical-Thermal-Analysis

Dynamic Mechanical Thermal Analysis (DMTA) is used to determine the material behavior of the elastomer components used as a function of frequency and temperature. The material is subjected to a sinusoidal stress that changes over time at constant temperature and different frequencies and the resulting material responses are measured. The stresses and distortions that occur are determined by the deformation or force change and are related to each other as described above.



Figure 9: principle of operation of the DMTA (left) and GABO 'EPLEXOR' (right), from [9]

The decisive material parameter, which is determined using the DMTA analysis, is the complex module  $E^*$ , as already described in Chapter 3.3. In Figure 9 a sketch of the principal operation as well as a picture of the DMTA machine at the University of German Armed Forces Munich is given.

Table 2: Parameter of DMTA – Temperature-Frequency Sweep

Sample	sliding bearing NR	sliding spring CR
Sample geometry [mm]	Rectangle: $L \times W \times T$ : 30 x 8.17 x 1.45	Rectangle: $L \times W \times T$ : 30 x 7.73 x 1.87
Test equipment	Eplexor 2000N Netzsch Gabo	
Test mode	Temperature- Frequency-Sweeps in Tension	
Temperature program [°C]	+100 : -100 (cooling)	
Temperature steps [°C]	5	5
Frequency program [Hz]	1.000; 1.968; 3.873; 7.622; 15.000	
Incitation stress [MPa]	1.10	0.60
Static stress [MPa]	1.60	1.60

In practice, DMTA testing machines are used to perform isothermal frequency sweep tests to obtain the complex modules within a limited frequency range at constant temperature, heat or cool the machine to the planned test temperature and repeat the frequency sweep.

The DMA experiments were performed on rectangular specimen, sweeping across five different frequencies (logarithmically equidistant spaced in the range of  $f \in [1; 15] \text{ Hz}$ ). For each frequency three load cycles were applied to the specimen. After the set of 15 cycles was completed the testing was repeated at the next testing temperature until the complete temperature program was done. The tests were performed stress-controlled. During the test the temperature was lowered with a rate of  $2^\circ\text{C}/\text{min}$  from  $+100^\circ\text{C}$  to  $-100^\circ\text{C}$  in steps of  $5^\circ\text{C}$ . At the beginning of the analysis the temperature was equilibrated at  $100^\circ\text{C}$  and held isothermal for 5 minutes. Table 2 contains the parameters used for the temperature-frequency-sweeps within the DMTA.

In Fig. 10 the raw data for the Storage and Loss modulus for the spring rubber are shown in dependence of the frequency and temperature range.

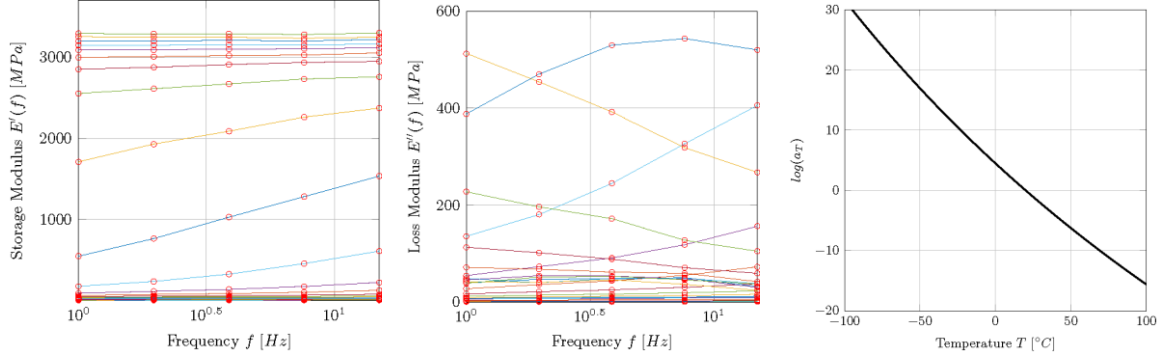


Figure 10: Isothermal Storage and Loss modulus curves within the tested frequency domain (left and middle) and horizontal shift factors over temperatures (right) for the sliding spring rubber

The Master Curve for a reference temperature of  $T_{ref} = 20^\circ\text{C}$  was obtained by horizontally shifting the data on the frequency axis, using the method ‘GUSTL’ and a Global Search method, both are described in [10]. The horizontal shift factors  $a_T$  were assumed to follow a TTSP of the Williams-Landel-Ferry (WLF) form. The TTSP parameters were obtained and the constraint  $\log(a_T) = 0$  at  $T = T_{ref}$ . The obtained Master Curve for the Storage modulus and for the Loss modulus is shown in Figure 11.

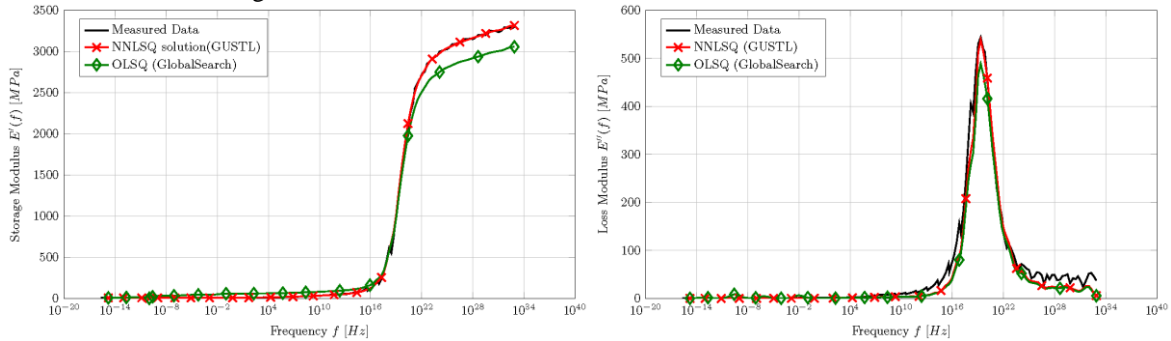


Figure 11: Storage Modulus Master Curve (left) and Loss Modulus Master Curve (right) for the sliding spring chloroprene rubber

The resulting Storage and Loss moduli obtained with ‘GUSTL’ in comparison to the ordinary Least-Squares approximation using the Global Search method shows, that ‘GUSTL’ fits the data more well and has a more smooth distribution of the coefficient  $E_i$  than the Global Search method. The distribution of the Prony-coefficient  $E_i$  is given in Figure 12.

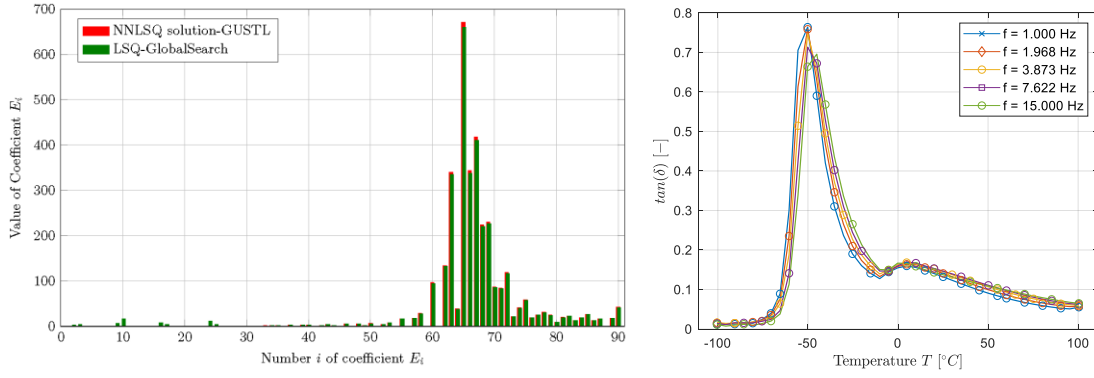


Figure 12: Prony-coefficients  $E_i$  (left) and Loss factor  $\tan(\delta)$  (right) for the sliding spring chloroprene rubber

Inspection of the Loss factor graph, given on the right in Figure 12, leads to the conclusion that the maximum damping occurs in the range of  $-50^\circ\text{C}$ , where also the Glass Transition region lies. Swivel joint expansion joints are exposed to a temperature range of  $-5$  to  $25$  degrees in bridges. With regard to the damping behavior, it is worth optimizing the polymer chemistry for an adaptation of the glass transition region, which represents the maximum damping.

In Fig. 13 the raw data for the Storage and Loss modulus for the sliding bearing rubber are shown in dependence of the frequency and temperature range.

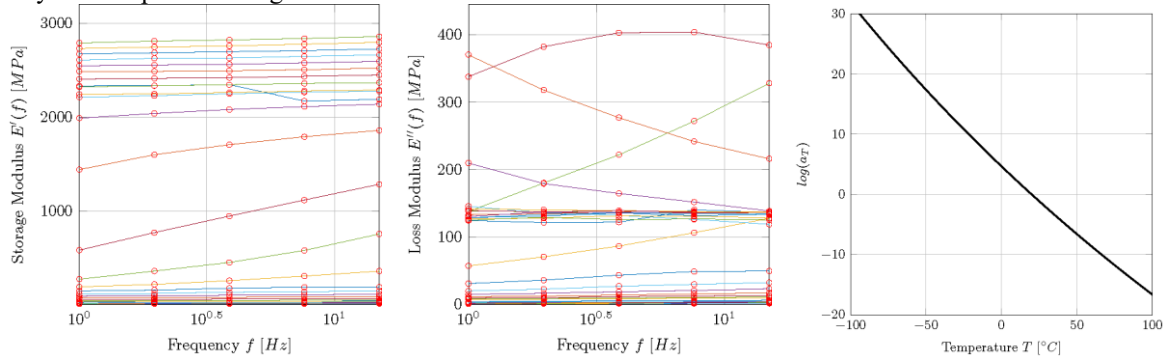


Figure 13: Isothermal Storage and Loss modulus curves within the tested frequency domain (left and middle) and horizontal shift factors over temperatures (right) for the sliding bearing natural rubber

The Master Curve for a reference temperature of  $T_{ref} = 20^\circ\text{C}$  was obtained by horizontally shifting the data on the frequency axis, again using the method ‘GUSTL’ and a Global Search method as described in the previous section. The horizontal shift factors  $a_T$  were assumed to follow a TTSP of the Williams-Landel-Ferry (WLF) form. The TTSP parameters were obtained under the constraint  $\log(a_T) = 0$  at  $T = T_{ref}$ . The obtained Master Curves for the Storage and Loss modulus for the sliding bearing are shown in Figure 14.

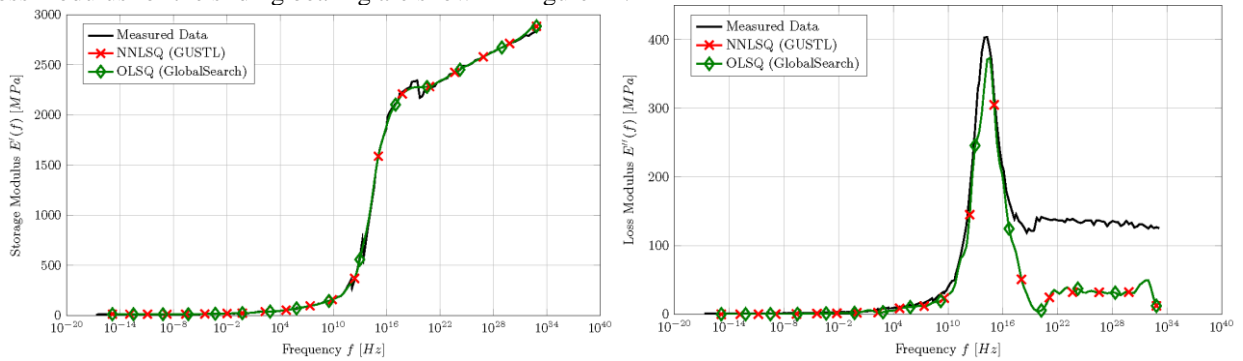


Figure 14: Storage Modulus Master Curve (left) and Loss Modulus Master Curve (right) for the sliding bearing natural rubber

The resulting Storage and Loss moduli obtained with ‘GUSTL’ in comparison to the ordinary Least-Squares approximation using the Global Search method shows, that ‘GUSTL’ fits the data more well and has a more smooth distribution of the coefficient  $E_i$  than the Global Search method. The distribution of the Prony-coefficient  $E_i$  is given in Figure 15.

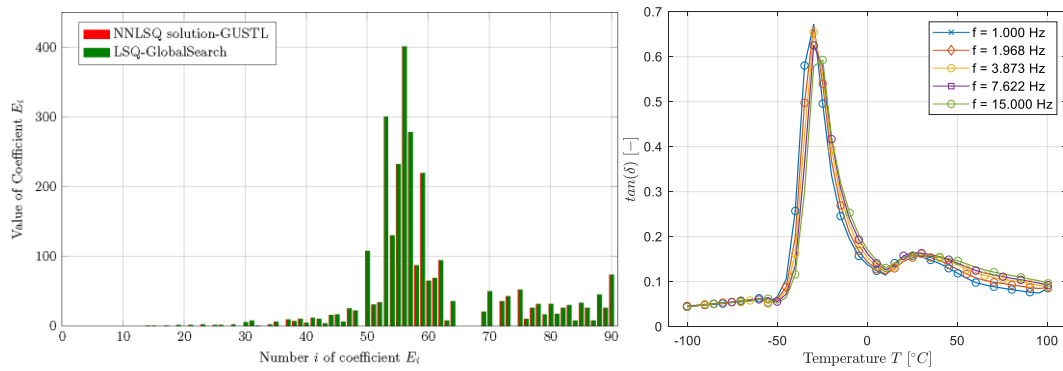


Figure 15: Prony-coefficients  $E_i$  (left) and Loss factor  $\tan(\delta)$  (right) for the bearing rubber

Here again, an inspection of the Loss factor graph, given on the right in Figure 15, leads to the conclusion, that the maximum damping occurs in the range of  $-45^\circ\text{C}$ , where also the Glass Transition region lies. Like the sliding spring, the sliding bearing is also exposed to a temperature range of  $-5$  to  $+25$  degrees. Below the glass transition from a temperature range of approx.  $0.0$  degrees, the damping behavior of both bearings is relatively constant. The vertical and horizontal transmission of force between the lamella and the crosshead is effected by a displacement and torsionally elastic bearing via the pretensioned plain bearing, from where the forces are transmitted into the structure via the traverse. Furthermore, the principle of these swivel joints is also used in earthquake areas. The primary stress results from dynamic influences, so it may be useful to change the polymer chemistry with regard to the maximum damping behavior, if possible in order to obtain the maximum damping.

Based on the conducted DMTA tests, the glass transition regions are estimated. The glass transition temperature  $T_g$  can be determined with various approaches, which may deliver significantly different results. Hence, it is more valuable to specify a glass transition range rather than a specific temperature. Figure 15 shows the evaluation approaches standardized in [11]. Accordingly,  $T_g$  can be determined either as the maximum of the loss modulus  $E''$  or the  $\tan(\delta)$ , as a turning point or in the "onset" of the storage modulus  $E'$ . Figure 15 only depicts the identification of the glass transition ( $\alpha$  - relaxation), all further relaxation processes are determined analogously by the further local maxima of the loss factor  $\tan(\delta)$  and the turning point of  $E'$ .

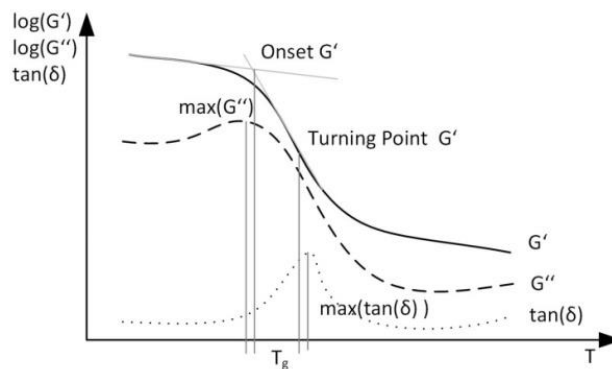


Figure 15: Definition of Glass transition temperatures  $T_g$

The results of the DMTA experiments and glass transition evaluation for the sliding key as well as the sliding bearing according to different methods in [11] are summarized in Table 3.

Table 3: Evaluation of the DMTA test results with respect to the Glass Transition Temperature

Sample		Sliding bearing NR	Sliding spring CR
$T_g$ [ $^\circ\text{C}$ ]	$\tan(\delta)$	-30	-50
	$\log G^* $	-35	-57

Comparing Figure 11 and Figure 14, there is a significant difference in the temporal behavior under isothermal conditions, since the reduction in stiffness of the chloroprene rubber sliding spring is achieved more quickly than that of the natural rubber sliding bearing. This different material behavior results in the expansion joint are being damped to a different maximum depending on the excitation frequency. This different behavior is now modeled as accurate as

possible in further finite element simulations in order to analyze the dynamic behavior of the expansion joint with realistic traffic loads. In upcoming simulations, the frequency-dependent material behavior determined here will be taken into account in order to establish the global damping behavior of the joint. Each component, especially the elastomer elements, with their thermal and frequency-dependent properties is modeled with the aid of rheological elements. The following tables show the approximated Prony series for the slide bearing (left) and slide spring (right), since the complete representation of the ninety row Prony series would exceed the content of the present work.

Table 4: Approximated Prony Series for the slide bearing (left) and the slide spring (right)

WLF Constants	$C_1$	151,22	WLF Constants	$C_1$	192,16
	$C_2$	694,95		$C_2$	844,85
	$T_0$ [°C]	20		$T_0$ [°C]	20
Young's Moduli [N/mm <sup>2</sup> ]	$E_0$	3,30E+03	Young's Moduli [N/mm <sup>2</sup> ]	$E_0$	2,84E+03
	$E_\infty$	0,0021		$E_\infty$	0,0047
$i$	$E_k / E_0$	Relaxation time $\tau_{ref,k}$ [s]	$i$	$E_k / E_0$	Relaxation time $\tau_{ref,k}$ [s]
1	1,6969E-04	1,0000E+05	1	1,3057E-03	1,0000E+05
2	3,8204E-04	1,5849E+01	2	5,0348E-03	2,1544E+00
3	1,5395E-03	2,5119E-03	3	1,8301E-02	4,6416E-05
4	3,1400E-03	3,9811E-07	4	2,3099E-02	1,0000E-09
5	4,9237E-03	6,3096E-11	5	1,0366E-02	1,0000E-10
6	1,0036E-02	1,0000E-14	6	6,8952E-05	2,5809E-11
7	5,7802E-03	1,0000E-15	7	3,4237E-02	6,6608E-12
8	1,1959E-02	1,7013E-16	8	1,0131E-02	1,7191E-12
9	1,7645E-02	2,8943E-17	9	3,5308E-02	4,4367E-13
10	4,0012E-02	4,9239E-18	10	8,8327E-02	1,1450E-13
11	1,1232E-01	8,3768E-19	11	6,9082E-02	2,9552E-14
12	1,4819E-01	1,4251E-19	12	1,2746E-01	7,6270E-15
13	2,1561E-01	2,4245E-20	13	1,4560E-01	1,9684E-15
14	1,4061E-01	4,1246E-21	14	4,6772E-02	5,0802E-16
15	8,3460E-02	7,0170E-22	15	7,3781E-02	1,3111E-16
16	4,3146E-02	1,1938E-22	16	4,1324E-02	3,3839E-17
17	4,0418E-02	2,0309E-23	17	2,4089E-02	8,7333E-18
18	1,4939E-02	3,4551E-24	18	2,6280E-02	2,2539E-18
19	1,9590E-02	5,8780E-25	19	2,1421E-02	5,8171E-19
20	1,1426E-02	1,0000E-25	20	2,3253E-02	1,0000E-21
21	2,1045E-02	1,0000E-26	21	3,6227E-02	6,3096E-24
22	1,3422E-02	3,1623E-28	22	3,7159E-02	3,9811E-26
23	1,7105E-02	1,0000E-29	23	3,4638E-02	2,5119E-28
24	1,1359E-02	3,1623E-31	24	3,3243E-02	1,5849E-30
25	1,4167E-02	1,0000E-32	25	3,8924E-02	1,0000E-32

## 5 Conclusion and Outlook

Many materials in modern civil engineering applications are polymer-based, which are showing distinct viscoelastic behavior. Thus in the whole design process the temperature and rate (time) dependence has to be considered as design or limiting parameters. In this paper the main theoretical foundation of hyperelasticity and viscoelasticity in both, the time and frequency domain, have been shown. The DMTA was introduced as a very handy method for the experimentally efficient determination of viscoelastic material properties. It was shown the experimental conduction of uniaxial compression tests as well as the deduced stiffness's of the sliding key as well as the sliding bearing under special consideration of stress softening (Mullins effect). A further experimental determination of the thermoviscoelastic properties of both, sliding key as well as the sliding bearing, was conducted using the DMTA.

The previous global damping behavior of the joint was determined on the basis of the decay behavior using the dimensionless damping factor; the Prony series must now be reduced by the damping factor in order to reflect the real behavior in the FE calculations. With the data now obtained, further theoretical calculations can now be carried out to improve the dynamic behavior with regard to fatigue. With the stochastically collected traffic data from further work drive-over simulations with different speeds and truck types are now planned in order to analyze the behavior of the joint on the basis of realistic dynamic loads. Finally, we would like to thank Maurer SE for their support in providing the test samples.

## 6 References

- [1] Nowak, Marcel und Fischer, Oliver. Site-specific fatigue demands on existing bridges based on local traffic data. Proceedings des 11. Deutsch-Japanisches-Brückenbau-Symposium . 2016
- [2] Tschoegl, Nicolas. The Phenomenological Theory of Linear Viscoelastic Behavior - an Introduction. Berlin : Springer-Verlag, 1989
- [3] Wrana, C.: Polymerphysik, Springer Spektrum 2014
- [4] Marques, Severino und Creus, Guillermo. Computational Viscoelasticity. Berlin : Springer, 2012.
- [5] Brinson, Hal F. ; Brinson, L. Catherine: Polymer Engineering Science and Viscoelasticity : An Introduction. 2. Aufl.. Berlin, Heidelberg: Springer, 2015.
- [6] Findley, William N. ; Davis, Francis A.: Creep and Relaxation of Nonlinear Viscoelastic Materials. Revised ed.. New York: Courier Corporation, 2013.
- [7] Lichte, U., Klimatische Temperatureinwirkungen und Kombinationsregeln bei Brückenbauwerken, Universität der Bundeswehr München - Institut für Konstruktiven Ingenieurbau, Dissertation, 2004
- [8] Knabenschuh, H., Bericht der Bundesanstalt für Straßenwesen, Temperaturunterschiede an Betonbrücken, Brücken- und Ingenieurbau Heft B 3
- [9] Halm, H., Deckmann, H.: Dynamic-Mechanical Thermal Analysis of Polymers and Solids, GABO brochure
- [10] Kraus, M.A., Niederwald, M.: Generalized collocation method using Stiffness matrices in the context of the Theory of Linear viscoelasticity (GUSTL). Tech. Mech. 37, Vol. 1, 82 - 106.
- [11] DIN EN ISO 6721-1: Kunststoffe – Bestimmung dynamisch-mechanischer Eigenschaften-Teil 1: Allgemeine Grundlagen - Deutsche Fassung. In. (2011)
- [12] DIN\_7724: Polymere Werkstoffe – Gruppierung polymerer Werkstoffe auf-grund ihres mechanischen Verhaltens. In. (1993)
- [13] Schwarzl, P.D.F.R.: Polymermechanik. Springer Verlag, Berlin, Heidelberg, New York (1990)
- [14] Schneider, J., Kuntsche, J., Schula, S., Schneider, F., Wörner, J.-D.: Glasbau - Grundlagen, Berechnung, Konstruktion. vol. 2. Springer, (2016)
- [15] Mullins, L.: Effect of stretching on the properties of rubber, J. Rubber Res., 16 (1947), pp. 275-289
- [16] Friedl, R.: Grundlagenorientierte theoretische und experimentelle Untersuchungen zum Schwingungsverhalten einer modifizierten Schwenktraversendehnfuge sowie zu fahrbahnunebenheitsinduzierten Radkraftschwankungen von Straßenfahrzeugen im Hinblick auf die daraus resultierende Streuung messtechnisch erfasster Fahrzeuggewichte, Dissertationsschrift, Universität der Bundeswehr München, München, 2017
- [17] MAURER SÖHNE: Maurer Schwenktraversen-Dehnfugen Produktbeschreibung; Bauwerksschutzsysteme
- [18] Mangerig, I., Friedl, R., Butz, C., „FE 88.0110/2011 bis FE 88.0112/2011 “IFuLa - Intelligenten Kalottenlager und intelligente Schwenktraversen-Dehnfuge”, BAST, 2016